UNIVERSITY OF LEEDS

This is a repository copy of *Reuse of UK alum water treatment sludge in cement-based materials*.

White Rose Research Online URL for this paper:
https://eprints.whiterose.ac.uk/168997/

Version: Accepted Version

Article:
Shamaki, M, Adu-Amankwah, S and Black, L orcid.org/0000-0001-8531-4989 (2021) Reuse of UK alum water treatment sludge in cement-based materials. Construction and Building Materials, 275. 122047. ISSN 0950-0618

https://doi.org/10.1016/j.conbuildmat.2020.122047

© 2020 Elsevier. This manuscript version is made available under the CC-BY-NC-ND 4.0 license http://creativecommons.org/licenses/by-nc-nd/4.0/.

Reuse
This article is distributed under the terms of the Creative Commons Attribution-NonCommercial-NoDerivs (CC BY-NC-ND) licence. This licence only allows you to download this work and share it with others as long as you credit the authors, but you can't change the article in any way or use it commercially. More information and the full terms of the licence here: https://creativecommons.org/licenses/

Takedown
If you consider content in White Rose Research Online to be in breach of UK law, please notify us by emailing eprints@whiterose.ac.uk including the URL of the record and the reason for the withdrawal request.

White Rose university consortium
Universities of Leeds, Sheffield & York

eprints@whiterose.ac.uk
https://eprints.whiterose.ac.uk/

Reuse of UK alum water treatment sludge in cement-based materials

Mubarak Shamaki, Samuel Adu-Amankwah, Leon Black*

School of Civil Engineering, University of Leeds, Woodhouse Lane, Leeds LS2 9JT, UK

* corresponding author: l.black@leeds.ac.uk

Abstract

Alum salts are commonly used as coagulants in the purification of surface water for potable supplies. The resultant waste alumina-rich sludge is currently landfilled in the UK. This study aimed to valorise sludge by using heat-treated alum sludge as an additive in cement. Alum sludge was calcined at 475-1100°C and then characterized to correlate physical and mineralogical changes with cementitious activity and engineering performance. Alum sludge calcined at 825°C transforms to poorly crystalline η-alumina (eta) and has cementitious activity. The calcined sludge rapidly reacts with gypsum to form ettringite which leads to a shortening of the induction period and onset of alite hydration. Gypsum depletion leads to undersulfated C_3A hydration which consumes ettringite to form monosulfoaluminate thereby inhibiting further alite hydration. The poorly crystalline η-alumina is metastable, transforming to highly crystalline α-alumina at 1100°C. In pastes containing more crystalline sludges, alite hydration is enhanced because the undersulfated C_3A reactions are avoided, leading to improved performance.

Keywords: Pozzolanic activity; Water Treatment Sludge

1. Introduction

Conventional supplementary cementitious materials (SCMs), such as ground granulated blast furnace slag and fly ash, are viable partial replacements for Portland cement. However, their limited availability in some locations, plus threats to global supply by, for example, the move away from burning coal for electricity generation, hinders their continued widespread use. This has motivated researchers to focus on finding new SCMs. The benefits of using industrial by-products and waste materials in cement-based materials are threefold; (i) environmental benefits from reduced abiotic depletion, waste avoidance, energy savings and lower CO_2 emissions ii) economic benefits from the use of lower cost construction materials and iii) technological improvement in rheological and mechanical properties of mortars and concretes.

The treatment of raw water for potable supplies involves a coagulation/flocculation process where chemical coagulants are used to agglomerate impurities, aiding sedimentation and filtration of the contaminants from the liquid phase. Aluminium sulfate is commonly used in the UK as a coagulant for the treatment of surface water [1]. Solid aluminium sulfate is added to water and is hydrolysed to form an amorphous or poorly crystalline gelatinous precipitate of aluminium hydroxide. This precipitate flocculates colloidal and suspended impurities such that they sink and can be removed. The resulting waste is an alumina-rich residue known as alum water treatment sludge (AWTS). The most common long-term disposal method for water treatment sludge is landfilling but this is actively being discouraged due to limited landfill spaces and increasing landfill costs. The physical and chemical characteristics of AWTS mainly depends on the dosage of coagulants added during the water

treatment process and the source water characteristics which is influenced by the catchment bedrock minerals and any impurities discharged into the river [2]. The variability in raw water quality is responsible for differences in the characteristics of AWTSs from one treatment plant to another and even for a specific plant from time to time [3]. Thus, due to variability in source water quality and treatment processes, it is necessary to characterize AWTSs from each water treatment plant (WTP) for recycling and reuse purposes.

In view of the aforementioned problems in dealing with AWTS, a few studies have attempted to valorize it in building and construction materials. AWTS has been considered for use as an SCM in concrete [4–7], in manufacturing aggregates [8–10] and in the production of cement [11]. Rodriguez et al. [12] reported that the substitution of 10-30% of cement with spray-dried water treatment sludge led to a significant reduction in compressive strength, with 28-day strengths reduced by 50-70%. Hydration was also retarded, affecting setting times of standard mortars.

AWTS usually contains clay minerals that can be dehydroxylated when heated between 700 and 850°C [13] yielding reactive alumina and silica. In turn, this induces pozzolanic reactions when incorporated in cement; improving strength and durability. Owaid et al. [4] studied the effect of AWTS calcined at 800°C on the mechanical properties of binary and ternary cement blends consisting of silica fume, ground granulated blast furnace slag and palm oil fuel ash. The binary blends with 15% calcined sludge produced higher compressive strength than the control mix, but further higher AWTS additions led to a gradual reduction in strength. Ternary blends showed better performance than binary mixes with identical AWTS substitution levels. Furthermore, Gastaldini et al. [6] determined that the optimum calcination conditions for improved reactivity was 700°C for 1 hour to achieve a 28-day strength activity index of 125%. Although the performance of calcined alum sludge has been reported, its hydration properties are unknown. It is assumed that the clay minerals present in source water and subsequent alum sludge are responsible for the improved performance.

This work investigates the potential reuse of calcined UK alum water treatment sludge as a supplementary cementitious material. Detailed chemical, mineralogical and physical characterization of raw and calcined AWTS as well as blended cement pastes and mortars has been conducted. The performance of calcined sludge was evaluated by means of testing the compressive strength of blended cement mortars. Based on obtained heat flow curves and characterization results, influences of calcined AWTS on the hydration of Portland cement provide a better understanding of the physical and chemical effect of calcined sludge. This work provides an important base for the widespread utilization of calcined alum water treatment sludge in the cement industry.

2. Materials and Methods

2.1. Materials

Mechanical testing was performed throughout this study on mortar samples, while pastes were used for mineralogical and microstructural characterization. A CEM I 52.5R cement, free from limestone, was used [14]. The fine aggregate was natural sand sieved to maximum size of 2 mm. An aqueous solution of modified polycarboxylate-based superplasticizer (Sika Viscocrete 25MP) was also used. The AWTS was collected from Elvington water treatment works located in York, United Kingdom. It was oven-dried at 105°C to constant mass. The dried sludge was then ground using a Retsch vibratory disc mill RS200 at 1300rpm for 5 minutes.

Calcined AWTS was prepared by placing oven-dried samples in a laboratory electric furnace and raising the temperature at a heating rate of 10°C/min followed by a holding time of 2 hours at target temperature. The calcined sludge was cooled gradually to ambient laboratory temperature and then ground using a Retsch vibratory disc mill RS200 at 1300rpm for 5 minutes. Selected samples are shown in Figure 1.

Figure 1. Physical appearance of a) As-received sludge; Ground Calcined sludge b) 825°C, c) 1100°C

2.2. Mix proportions and sample preparation

To evaluate the pozzolanic acitivity of calcined alum sludge, 50 mm mortar cubes prepared with different formulations, a binder/sand ratio of 1:3 and a water/binder ratio of 0.55 were used. Mortar mix proportions are shown in Table 1. Reduced workability due to calcined sludge fineness was mitigated by adding 1% superplasticizer by mass of total binder (sludge and cement). The sludge-cement blends were prepared at 20 wt% replacement. Binders were homogenized in a laboratory ball mill for at least 2 h using polymer balls to prevent further grinding. Mortars were mixed for 4 min using an automatic mixer compliant with BS EN 196-1 [15]. The mortar specimens were demolded after 24 hours and stored in a curing room at 95% relative humidity and 20°C until the test age.

Table 1: Mortar Mix Proportions

Mix description	w/b	Water (g)	Cement (g)	Alum Sludge (g)	Sand (g)	SP (%)	Mortar Flow (mm)
C	0.55	247.5	450	-	1350	1	232
CR	0.55	247.5	360	90	1350	1	172
C475	0.55	247.5	360	90	1350	1	131
C625	0.55	247.5	360	90	1350	1	144
C825	0.55	247.5	360	90	1350	1	118
C1000	0.55	247.5	360	90	1350	1	169
C1100	0.55	247.5	360	90	1350	1	228

The corresponding cement paste samples were hand-mixed, cast in 8ml plastics vials, vacuum-sealed and then stored in a water bath at 20°C until test age. Before testing, the paste samples were hydration stopped by solvent exchange with isopropanol and then washed with diethyl ether following the procedure described elsewhere [16].

2.3. Sample characterization

2.3.1 Physical Properties of alum sludge samples

Specific surface area was measured by the BET standard method [17]. Pore-size distributions were calculated from the desorption branch of the isotherm using the BJH method [18]. Particle size distribution and specific density were determined using laser diffraction and helium pycnometry respectively. A Zeiss EVO 15 scanning electron microscope was used for morphological analysis of raw and calcined sludge powders, with powder samples dispersed onto adhesive carbon pads and carbon coated prior to investigation. The instrument was operated in secondary electron mode and at 10 keV accelerating voltage.

Table 2. Physical properties of cement, raw sludge and calcined sludges

Physical Property	Cement	Raw alum sludge	Calcined at 475 ºC	Calcined at 625 ºC	Calcined at 825 ºC	Calcined at 1000ºC	Calcined at 1100ºC
Density (g/cm^3)	3.17	2.20	2.58	2.85	3.09	3.12	3.31
D_{50} (μ)	11.66	7.51	17.37	19.95	24.76	20.34	7.73
BET Surface area (m^2/g)	1.01	53.77	99.41	81.68	110.18	61.43	15.14
Total Pore Volume (cm^3/g)	-	0.199	0.345	0.395	0.533	0.401	0.220
Average Pore Diameter (nm)	-	10.04	9.06	13.30	13.78	19.45	44.40

2.3.2 Chemical and microstructural characterization of materials

The oxide compositions of raw and calcined sludge powders were determined by XRF spectroscopy from lithium tetraborate fused bead samples and expressed in terms of oxides (Table 3),.

Table 3. Chemical composition of cement, raw sludge and calcined sludge

Chemical composition	Cement	Raw alum sludge	Calcined sludge at 825 ºC	Calcined sludge at 1000ºC	Calcined sludge at 1100ºC
SiO_2	20.50	10.28	17.67	18.93	19.09
Al_2O_3	4.60	44.24	67.38	68.40	68.29
Fe_2O_3	2.40	2.51	4.75	4.83	4.74
CaO	63.40	2.50	4.55	4.72	4.79
MgO	2.00	0.34	0.53	0.46	0.49
SO_3	3.60	1.24	2.12	0.08	0.05
Na_2O	0.13	0.15	0.75	0.76	0.80
P_2O_5	0.30	0.44	0.77	0.78	0.76
MnO	0.00	0.15	0.30	0.30	0.30
TiO_2	0.30	0.16	0.34	0.31	0.24
K_2O	0.74	0.43	0.76	0.76	0.80
LOI 950ºC	1.50	36.4	-	-	-
Total		98.84	99.92	100	100

SEM analysis of hydrated cement pastes was performed to understand microstructural development. Slices were cut at test age, hydration stopped, resin impregnated, polished and carbon coated prior to analysis. 25 back-scattered images (BSE) per sample were analyzed quantitatively to determine the cement paste coarse porosity. EDX analysis was applied to determine C-S-H composition [19], with data from at least 100 points per sample. Inner product C-S-H was sampled to minimize intermixing with other phases.

Thermal analysis was used to characterize uncalcined alum sludge and blended cement pastes. This was carried out using about 30mg samples under nitrogen. The heating rate was 5°C/min and 10°C/min for the raw sludge and cement pastes respectively. STA data (Figure 2) was used for the selection of subsequent calcination temperatures. A LECO furnace was used for the determination of inorganic and organic carbon (Table 4).

Table 4. Total carbon of raw and calcined sludges

	TOC (%)	Inorganic carbon (%)
Raw Sludge	9.72	0.59
475°C	0.39	0.20
625°C	0.13	0.11
825°C	0.07	0.02
1000°C	-	-
1100°C	-	-

In cement pastes, portlandite (CH) contents were determined by the weight loss between 380 and 500°C, using the tangent method [20]. A correction to the portlandite content was made to account for the amount of carbonated CH which can be detected in the decarbonation process between 600 and 900°C [21]. The total portlandite content was calculated using the following equation (1):

$$CH\% = \Delta CH \times M_{Ca(OH)2}/M_{H20} + \Delta CC \times M_{Ca(OH)2}/M_{CO2}$$

Where ΔCH is the weight loss due to dehydration of calcium hydroxide; ΔCC is the weight loss due to decarbonation of calcite; and $M_{Ca(OH)2}$, M_{H20} and M_{CO2} are the molar masses of portlandite ($74 g.mol^{-1}$), water ($18 g.mol^{-1}$) and carbon dioxide ($44 g.mol^{-1}$) respectively. The bound water content (W_n) was recognized as the mass loss between 50°C and 550°C normalized to the ignited mass at 550°C given by equation (2) [20]. This was then corrected for sample carbonation:

$$W_n = (W_{50^oC} - W_{550^oC}) / W_{550^oC}$$

where W_{50^oC} and W_{550^oC} is the sample mass after ignition at 50°C and 550°C respectively.

Powder X-ray diffraction was performed on Bruker D8 Advance X-ray diffractometer with a Cu Kα X-ray source, over a range 5–70° 2θ. Diffrac-Eva software with crystallography open database (COD) was used to identify the mineral phases present in the raw and calcined sludge samples. The XRD patterns of cement pastes were analyzed quantitatively using the X'pert Highscore Plus software with corundum as an external standard [20]. All structure models were taken from the ICSD library for Rietveld refinement (Table 5).

Table 5: Phase structure references used for Rietveld analysis.

Phase	Formula	Crystal structure	ICSD code
Alite	Ca_3SiO_5	Monoclinic	64759
Belite	Ca_2SiO_4	Monoclinic (β)	79550
Aluminate	$Ca_3Al_2O_6$	Cubic	1841
Aluminate	$Ca_3Al_2O_6$	Orthorombic	1880
Ferrite	Ca_2AlFeO_5	Orthorombic	51265
Gypsum	$CaSO_4 \cdot 2H_2O$	Monoclinic	409581
Calcite	$CaCO_3$	Trigonal	166364
Portlandite	$Ca(OH)_2$	Monoclinic	15471
Ettringite	$Ca_6Al_2(SO_4)_3 \cdot (OH)_{12} \cdot 26H_2O$	Hexagonal	155395
Monosulfoaluminate	$Ca_4Al_2(SO_4) \cdot (OH)_{12} \cdot 6H_2O$	Trigonal	100138
Corundum	Al_2O_3	Rhombohedral	73725

Sludge samples were also characterised using a Perkin Elmer ATR-FTIR spectrometer, over the range 400–4000 cm^{-1}, with a resolution of $4cm^{-1}$.

Isothermal calorimetry was performed using a TAM Air Calorimeter to determine how calcined sludge influences the initial cement hydration kinetics. Paste samples comprising 6g of binder and 3.36g stock solution of deionised water containing superplasticizer were mixed in plastic ampoules using a vortex shaker for 2 min and transferred into the calorimeter sample channels. Corresponding quartz reference samples were placed in the reference channels. Data were collected for 10 days.

2.3.3 Mortar Performance

The workability of fresh mortar was measured using a flow table in accordance with BS EN 1015-3 [22]. Compressive strengths of mortars were measured in accordance with ASTM C109 [23] at 2, 7 and 28 days of curing using a 3000 KN capacity ToniPact automatic compression test machine. The pozzolanic activity index of calcined sludges was evaluated in accordance with ASTM C618 [24].

3. Results and discussion

3.1. Thermal characterization of as-received AWTS

Figure 2 shows the TG/DTA thermograms of oven-dried sludge. The steady mass loss suggests multiple, overlapping decomposition steps, but with two main mass losses with temperature. Prior drying at 105ºC had removed most of the physically absorbed thus the residual free or unbound water was only about 2.2%, observed as the endothermic peak at 75ºC. There was ~31% mass loss over the temperature range 200ºC to 625ºC, due to dehydroxylation of $Al(OH)_3$ to alumina and the combustion of organic carbon [25–27]. These are denoted by the strong endothermic and exothermic peaks centered at 275ºC and 400ºC respectively. At 579ºC the α- to β-quartz transition was observed. β-quartz then remains stable up to 900-1000ºC [28]. An inflection centered at 789ºC in the DTA curve was accompanied by slight mass loss up to 1000ºC, and could be attributed to desulfurization [29,30]. The thermal analysis data defined the temperatures for heat-treating AWTS; namely 475, 625, 825, 1000 and 1100ºC. These temperatures lie between the end of combustion of organics and the beginning of the formation of α-alumina, the end product of $Al(OH)_3$ decomposition [31].

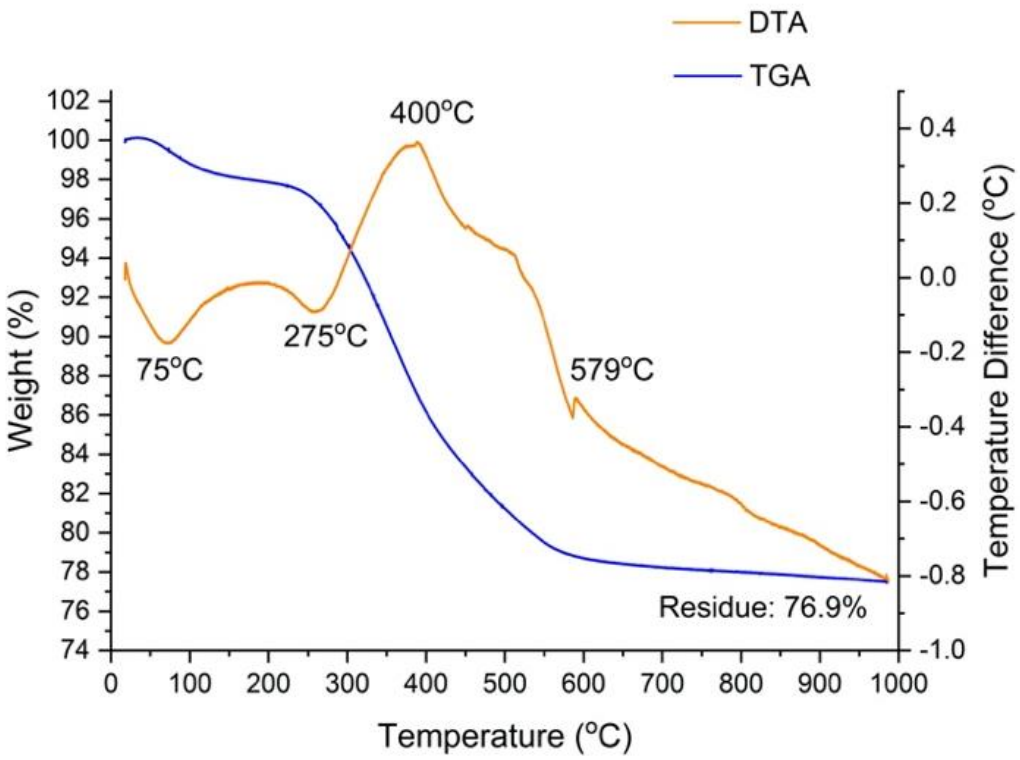

Figure 2. Thermal Analysis of raw sludge

Table 3 shows the chemical composition of raw and calcined sludges. Due to the removal of TOC and dehydroxylation of the alumina phases, there is significant enrichment of the residual phases present. The results show that the calcined sludge is composed primarily of aluminates.

The measurement of the organic carbon in waste materials is particularly important for reuse as SCMs, since organic carbon absorbs water and coats cement grains leading to a decrease in compressive strength [32]. In order to limit the unburnt carbon content in fly ash used as an SCM, BS EN 450 limits the loss on ignition value to a maximum of 9% [33]. The organic carbon contents (Table 4) fell upon calcination from 9.7% in the raw sludge to 0.39% at 475°C, in line with the assignment of the exothermic peak at 400°C being due to the combustion of organics. Organic carbon in AWTS originates from organic soils dissolved in water and flocculated by the alum added during the water treatment process [2].The inorganic carbon content in the raw sludge was 0.6% and was zero by 825°C.

3.2. Physical properties of raw and calcined AWTS

Pozzolanic activity of SCMs is not only influenced by chemical composition, but also physical properties, which are significantly modified by thermal treatment. Sludge calcined at different temperatures and then subjected to the same grinding regime showed systematic variations in density, specific surface area and particle size (Table 2). During the dehydroxylation/dehydration process, aluminium hydroxides suffer an intense mass loss, but with densification; generating internal pores. Mean particle sizes gradually increased with calcination temperature up to 825°C (Figure 3), attributed to sintering and agglomeration of the finest particles. At higher temperatures still finer particles were due to de-agglomeration as revealed by electron microscopy.

SEM images (Fig 6a-f) illustrate the influence of calcination temperature on particle morphology and possible mechanisms which produced the variation in particle size, BET surface area and pore characteristics (Table 2). At lower temperatures, particles were irregularly shaped with various sizes

and rough surface textures. No significant changes were observed at calcination temperatures up to 825°C, where maximum Specific Surface Area (SSA) and particle size was observed due to agglomeration. At 1000°C, sintering was observed as particle edges became more rounded with reduced surface roughness. This is consistent with the observed reduction in BET surface area. At 1100°C dehydroxylation and conversion to corundum was complete, leading to finer particles and a drastic reduction in SSA.

The trend in SSA and particle size distribution (PSD) can be explained by the nitrogen adsorption isotherms and pore size distributions (Figure 4 and 5). The BJH pore-size distributions indicate mesoporous materials. Calcination leads to an increase in surface area from 53.77 m^2/g (as-received) to 110 m^2/g at 825°C, and total pore volume from 0.199 to 0.533cm^3/g. Both surface area and pore volume decrease at higher temperatures, significantly between 1000°C and 1100°C. This process can be explained as: the raw sludge, an $Al(OH)_3$ gel, has a high water content. Dehydroxylation leads to rapid loss in mass without a reduction in external dimensions [31,34] and so formation of pores with a high internal surface area. Thus, the sludge calcined at 825^0C has the highest surface area. Collapse of pore walls upon heating at higher temperatures results in a decrease in pore volume [35]. In the 1000-1100°C temperature range, the surface area decreased significantly indicating first signs of sintering and formation of α-alumina [36]. The changes in physical properties are consistent with the literature [18,35,37]. Based on the variation in SSA, it is expected that upon blending with cement, the water demand will increase with calcination temperature up to 825°C and thereafter decline.

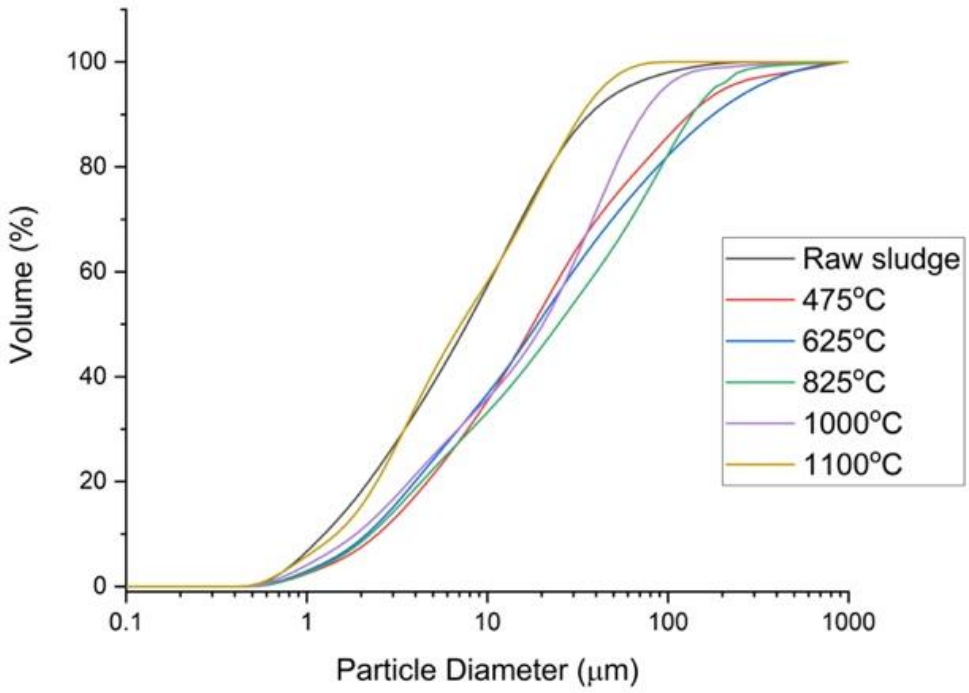

Figure 3. Particle size distribution of raw and calcined sludges

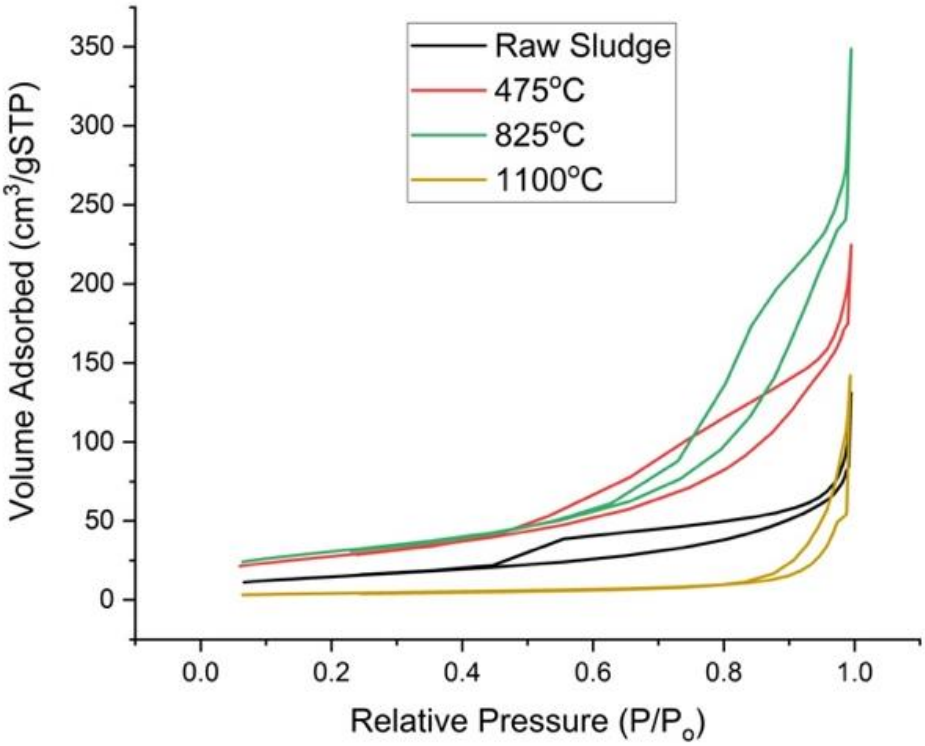

Figure 4: Nitrogen adsorption/desorption isotherms for raw and calcined sludges at 475, 825 and 1100 °C.

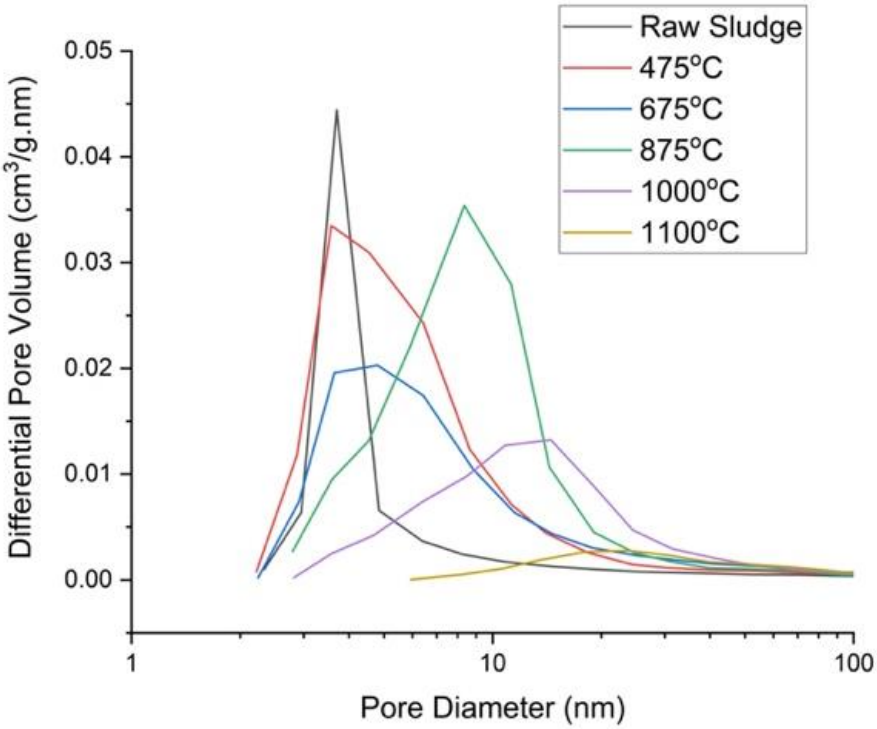

Figure 5. BJH pore-size distributions of raw and calcined sludges

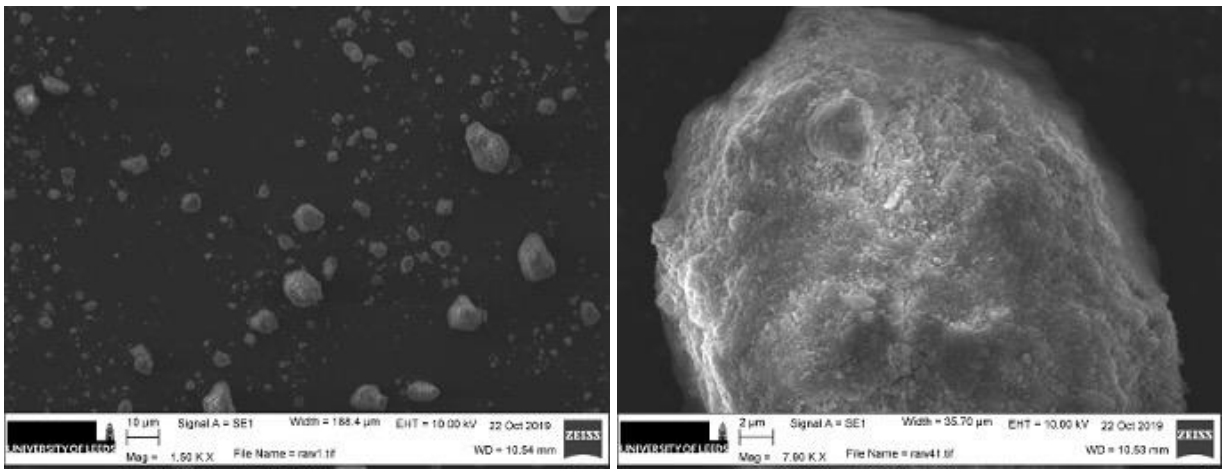

a) Ground raw sludge

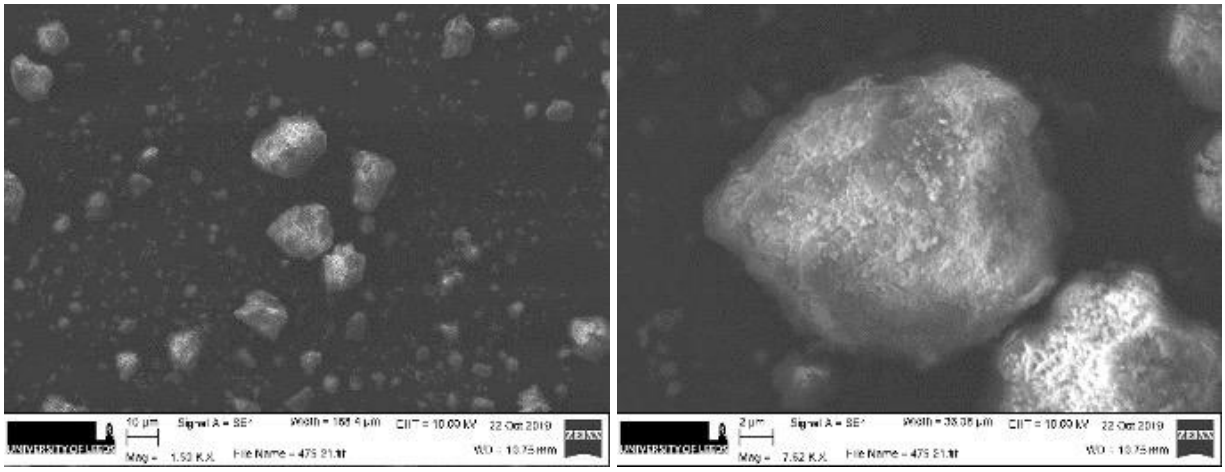

b) 475°C

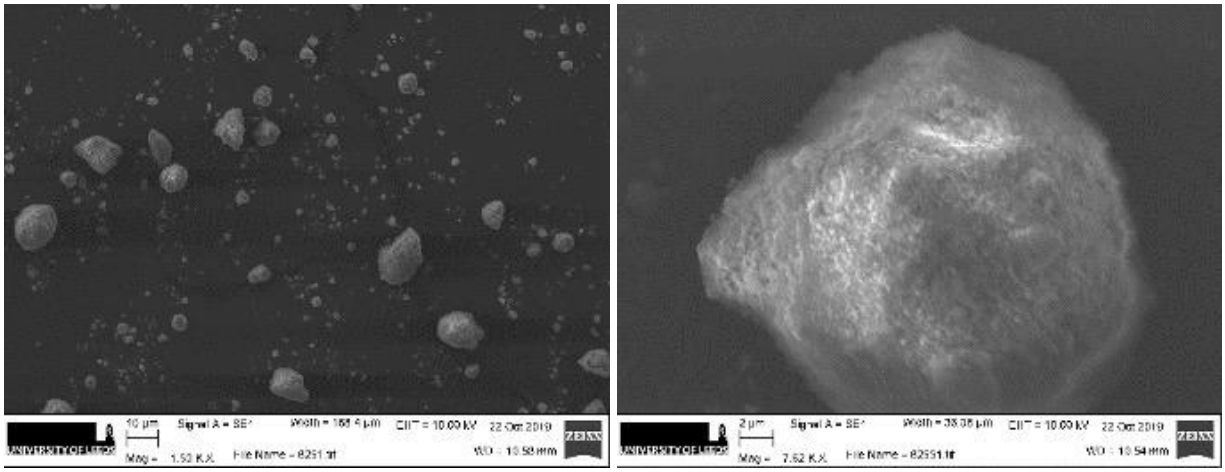

c) 625 °C

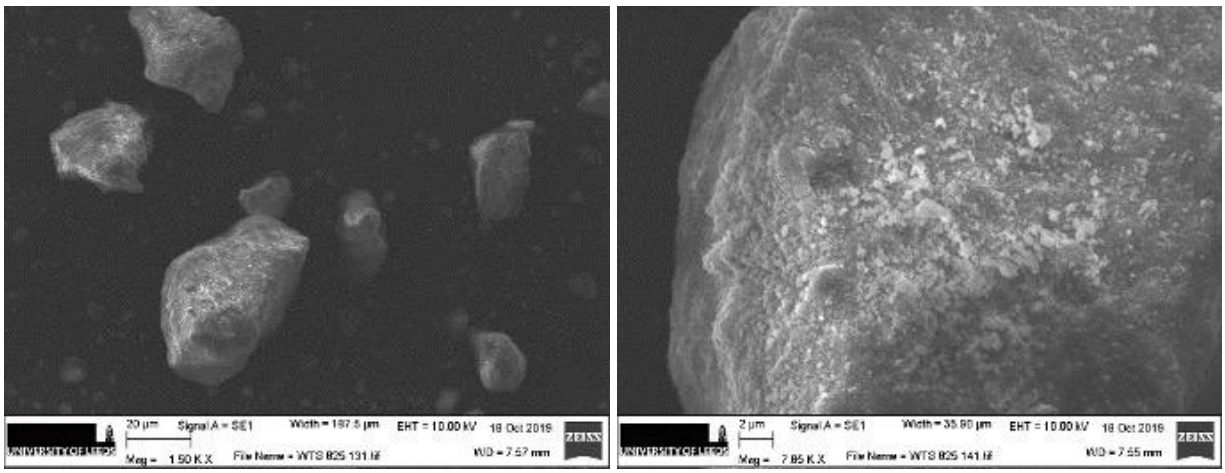

d) 825 ºC

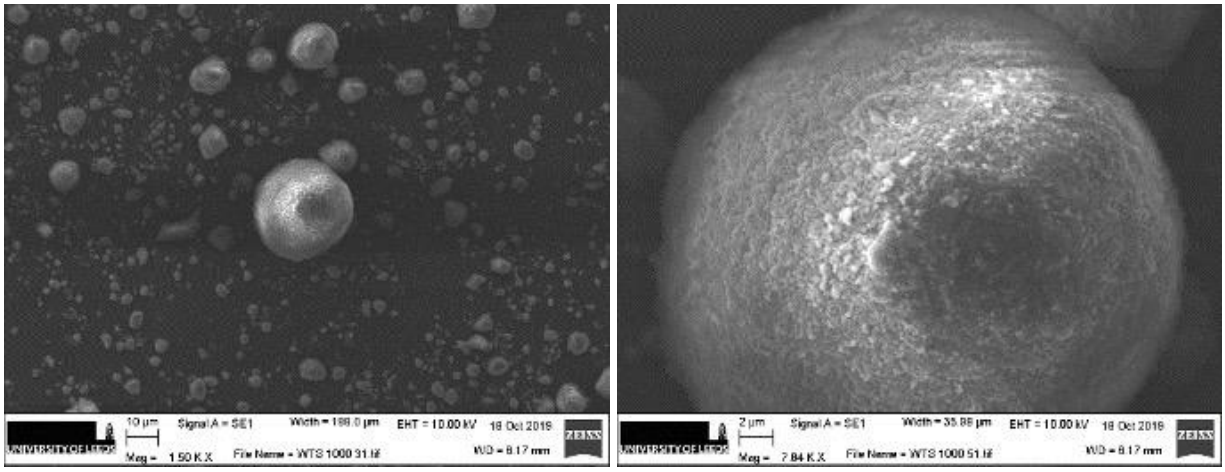

e) 1000 ºC

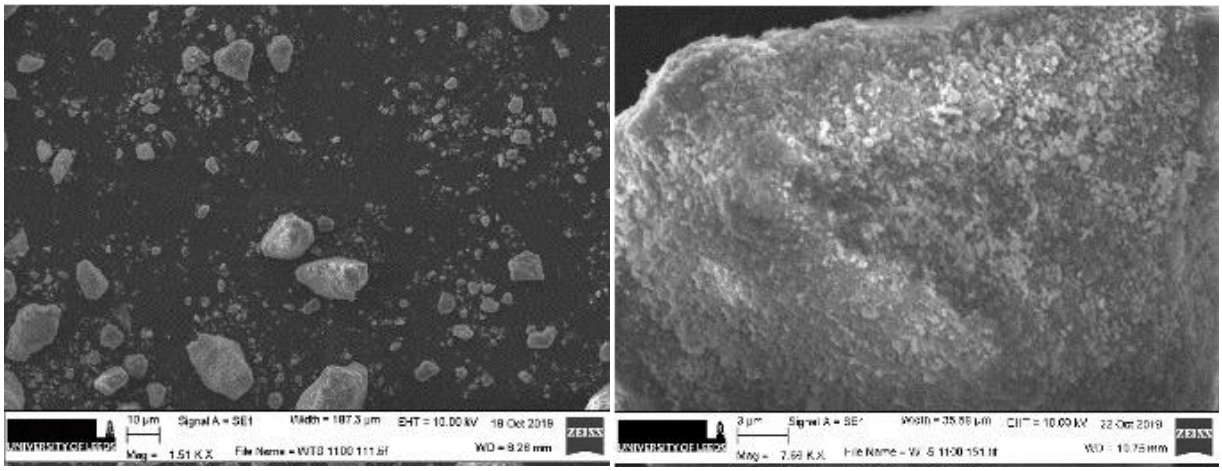

f) 1100 ºC

Figure 6: Secondary electron microscopy images of raw and calcined sludges

3.3. Mineralogical Characterization of AWTS samples

3.3.1 XRD Analysis

XRD patterns (Figure 7) show that the raw sludge was primarily amorphous, with quartz and montmorillonite the only crystalline phases detected. Heating to 475ºC and then 625ºC revealed no change in the crystalline composition, indicating that mass loss observed in STA was due to loss of

water and organic carbon. Only upon heating to 825ºC was there a noticeable change in crystallinity, with appearance of reflections due to η-alumina (eta). The formation of η-alumina is consistent with synthesis of aluminium hydroxide gels from aluminium sulfates [29,30]. By 1000ºC feldspar was detected, indicative of montmorillonite decomposition [13], and the η-alumina reflections become more prevalent. Similarly, gehlenite was formed arising from CaO plus reactive Al_2O_3 and SiO_2. On further heating at 1100ºC, the montmorillonite reflection disappeared while η-alumina transformed to alpha alumina, indicating complete dehydroxylation [38,39]. This occurs with the formation of another high temperature phase, mullite, from the reaction of silica- and alumina-rich phases in the sludge, suggesting the possible reaction of η-alumina with silica-rich phases. The thermal changes are consistent with previous studies on the thermal decomposition of clays and aluminium hydroxides [40–43].

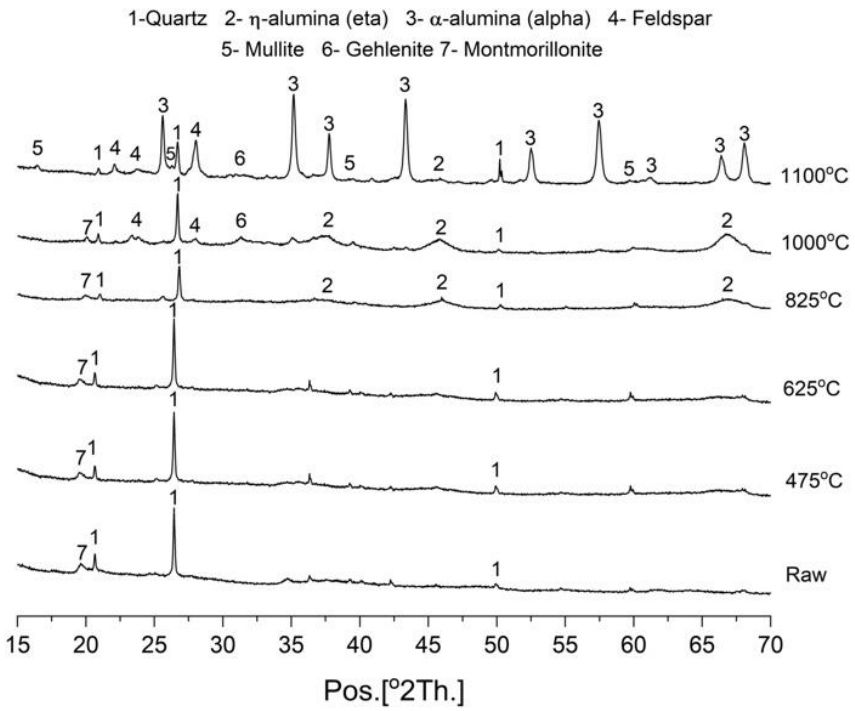

Figure 7: XRD of calcined sludge

3.3.2 FTIR Analysis

FTIR-ATR spectra are shown in Figure 8. The band at 1640 cm^{-1} may be attributed to H-O-H bending vibrations of interlayer water, while the broad band at 3340cm^{-1} is due to OH^- bonds of structural water present in $Al(OH)_3$ [44,45]. These bands decrease in intensity with increasing temperature indicating alumina dehydroxylation, finally disappearing by 1100ºC. This also coincides with the collapse of the montmorillonite structure as observed by XRD.

Very weak carbonate υ3 stretching bands at 1435cm^{-1} diminished with increasing temperature; disappearing by 825ºC. This is in line with known behaviour of calcite and loss of inorganic carbon as observed in TOC analysis (Table 4).

Bands due to the silica network are in the range 465-1150 cm^{-1} [25,26]. In the raw sludge, the intense Si-O stretching bands at 1030 cm^{-1} and 532 cm^{-1}, the bending band at 465 cm^{-1}, as well as the shoulder at 912 cm^{-1} are typical for smectite minerals [46,47]. The band at 912 cm^{-1} is attributed to Al-O-H deformation of the octahedral sheet in such structures. Peaks at ~532 and 465 cm^{-1} are assigned to Al-

O-Si and Si-O-Si deformations, the latter characteristic of amorphous silica. The presence of quartz is also confirmed by the band at 793 cm^{-1} [27,48].

Calcination at 475°C led to the disappearance of the Al-O-H band at 912 cm^{-1} as clay minerals dehydroxylated. The broad band at 1030cm^{-1} showed a shoulder at 1100cm^{-1} due to montmorillonite [47]. With increasing temperature, these bands transformed to a single absorption at 1100 cm^{-1} characteristic of amorphous reactive silica species [43,49]. At 825°C, a new band at 723cm^{-1} emerged due to Al-O-Al, with growth of this band as $Al(OH)_3$ transformed to an oxide [45]. Heating to 1100°C led to sharp and distinct peaks due to corundum (α-alumina) at 444 cm^{-1}, 487 cm^{-1}, 637cm^{-1} and 583 cm^{-1} [50], in agreement with the XRD patterns. The formation of mullite at 1100°C is indicated by the emergence of the broad band at 834 cm^{-1} [51], attributed to Si-O-Al linkages, again consistent with XRD analysis.

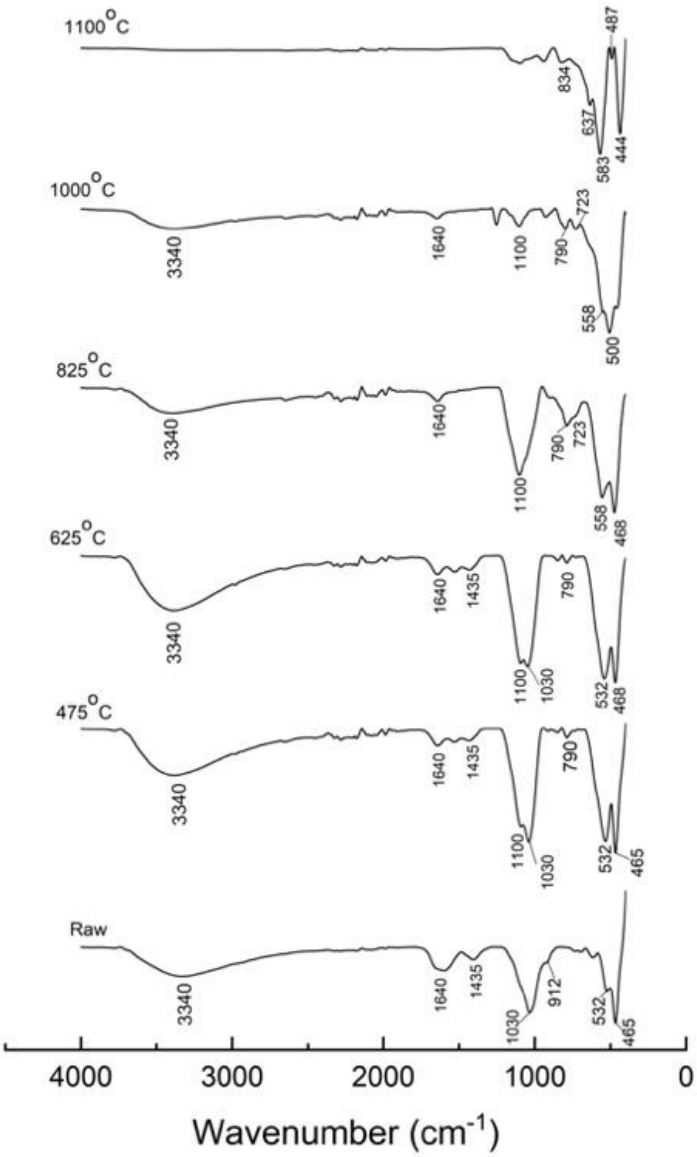

Figure 8: FTIR analysis of sludge samples

3.4. Influence of calcined sludge on hydration and microstructure of cement pastes

3.4.1 Isothermal Calorimetry

Figure 9 shows the calorimetric curves of neat OPC and calcined sludge-cement pastes normalized to OPC content. The cumulative heat curves indicate that the calcined sludges contribute both a filler

and chemical effect, with more crystalline sludges, namely those calcined at 1000ºC and 1100ºC, exhibiting a lesser chemical effect on OPC hydration. There was acceleration of the main hydration peak with increasing surface area (Table 2), due to increased nucleation sites.

All of the sludge blends show acceleration of the main hydration peak. For the sludges calcined at 1000 (C1000) and 1100ºC (C1100) acceleration was slight, but there was clear evidence of sludge reaction, seen in the increased total heat evolution (Figure 9b). The reaction was ever so slightly greater for the sludge heated at 1000ºC, likely to the inert nature of the corundum formed at 1100ºC. The sludge calcined at 825ºC (C825) showed a marked change in hydration behaviour from pure Portland cement. C825 contains significant quantities of reactive, amorphous aluminates. These led to significant shortening of the induction period. In addition, there was a high initial exotherm and a peak preceding the main hydration peak. The first exotherm is associated with ettringite formation, which induces rapid hardening and early set of cement pastes [52,53]. This was evidenced during mixing of cement pastes where the C825 paste solidified much faster than the others. The amount of ettringite formed during these very early stages is controlled by the concentration of Al^{3+}, C_3A content in cement and gypsum dissolution rate [54]. The rapid reaction between of $[Al(OH)_4]^-$ from the sludge and gypsum to form ettringite accelerates C_3A hydration. This rapid reaction is followed by the conversion of ettringite to monosulfate after about 3 hours [55]. Because C_3A reacts prior to the onset of silicate reaction, the C825 system is undersulfated [55,56]. Furthermore, the induction period of C825 paste is significantly shortened. This could be attributed to the rapid consumption of Ca^{2+} and SO_4^{2-} which expedites gypsum and alite dissolutions thereby accelerating the onset of the silicate hydration peak [54,57].

In C825, the main hydration peak was lower and broader. Although, the early AFt precipitation contributes to early space filling, the higher aluminate dissolution rate may limit alite hydration. Explanations for this behaviour include: covering of cement particles by the early formed monosulfoaluminate thereby hampering alite hydration [58]; formation of C-A-S-H, acting as a poor nucleation site for additional C-S-H [59]; stabilization of alite by aluminium [56]; or retardation of alite dissolution by the formation of Al-Si species interacting with alite surfaces [60]. The latter view is supported by experimental findings that suggest aluminium retards the dissolution of amorphous silica [61].

In pastes C1000 and C1100, a properly sulfated condition exists because C_3A hydration does not occur before the onset of the silicate hydration peak [56]. The higher crystallinity of the sludges in these mixes prevents the rapid consumption of $CaSO_4$ which delays C_3A hydration. This results in longer induction periods and increased alite hydration.

These observations section suggest a competition between silicate and aluminate reactions. C_3A reaction is significantly affected by calcined sludge, particularly the more amorphous sludge at 825ºC which contains higher hydratable Al^{3+} concentration. The composition of the calcined sludge is expected to have an effect on AFt and AFm formation, and alite hydration. This will affect mechanical strength development.

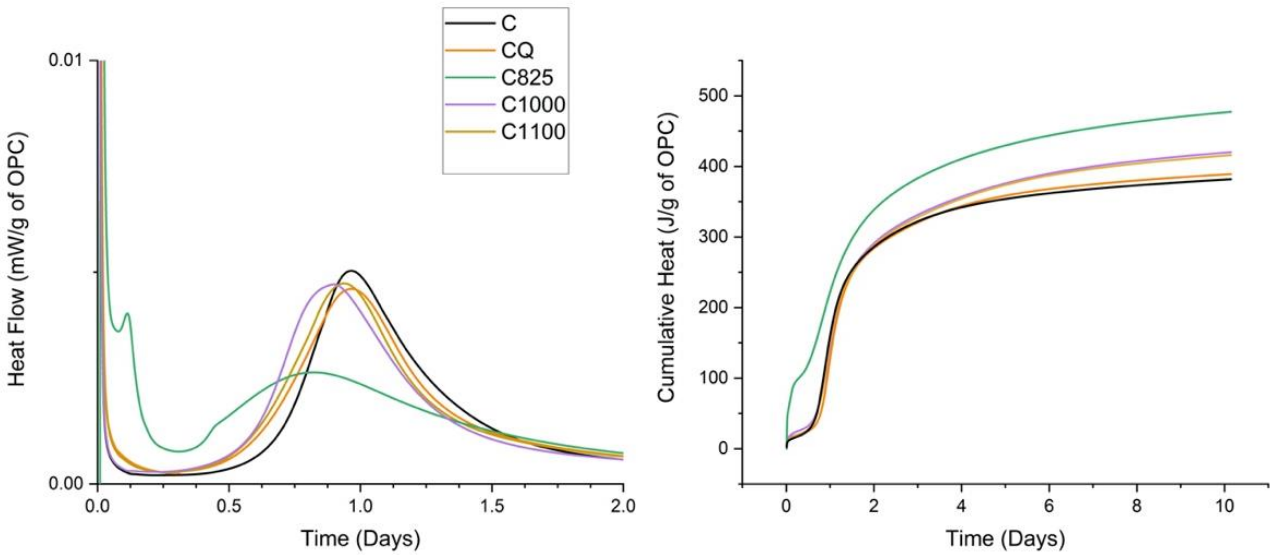

Figure 9: Calorimetric curves of Portland cement with 20% calcined sludge

3.4.3 Thermogravimetric Analysis

Figure 10 shows the TGA and DTG curves for all 28-day pastes, while Table 6 shows the amount of chemically bound water and CH contents. The traces show three prominent peaks; at about 100ºC due to the decomposition of ettringite and C-S-H; at about 190ºC from loss of structural water from AFm, and between 400ºC and 500ºC due CH dehydroxylation. The peaks above 600ºC are due to decarbonation of calcite due to carbonation of CH by atmospheric CO_2 and are an artefact of sample preparation. The peak due to AFm is most prominent in C825, then C1000, being related to the availability of reactive alumina. This is consistent with calorimetry results that indicate accelerated C_3A reaction with ettringite to form monosulfoaluminate from as early as 3 hours.

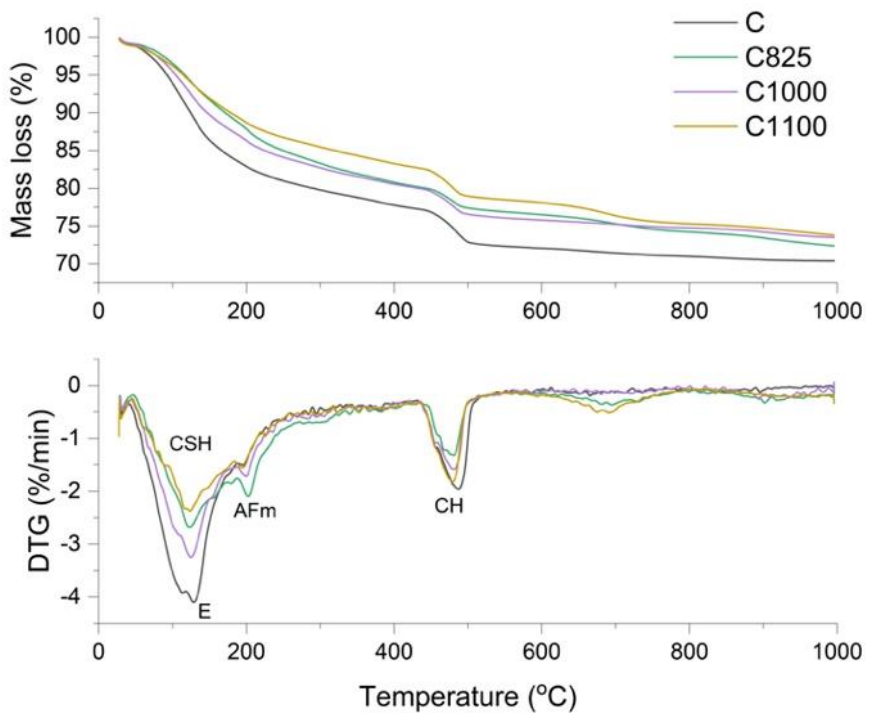

Figure 10: TG and DTG curves of cement pastes containing calcined sludge at 28 days curing.

Table 6: Weight % CH, bound water, clinker phases, AFt and AFm relative to anhydrous content

	Time (d)	C_3S	C_2S	C_3A	C_4AF	Ms	AFt	CH (TGA)	Bound water	DoH OPC
C	0	58	20	2.8	9.8					
	2	10	17.4	0.8	5.9	0.3	7.2	16.8	20.3	62.3
	7	6	15.1	-	5.2	1.3	8.2	17.3	30.6	70.9
	28	3.2	12.1	-	2.2	1.7	12	24.1	36.7	80.7
C825	0	46.4	16	2.2	7.8					
	2	16.5	15.4	-	5.1	1.4	12.7	13.1	30.9	48.8
	7	10.4	11.5	-	3.7	12.4	6.2	13.8	34.3	64.6
	28	8.5	9.2	-	1.2	21	3.6	12.6	36.8	73.9
C1000	0	46.4	16	2.2	7.8					
	2	13.4	15.2	0.4	5.6	0.6	11.9	15.7	27.9	52.2
	7	9.2	13.3	-	4.1	12.3	8.4	18.4	32.1	63.2
	28	5.1	8.2	-	1.1	13.7	5.7	13.8	37.7	80.1
C1100	0	46.4	16	2.2	7.8					
	2	8	14.9	0.7	4.5	0.07	11.8	15.9	26.7	61.2
	7	5.1	12.1	-	1.9	2.4	8.8	19.1	31.0	73.6
	28	0.7	9.2	-	0.7	10.2	4.8	19.9	33.5	85.3

C825 paste had the lowest CH content, consistent with calorimetry results where inhibition of alite hydration was observed. C1000 showed higher portlandite contents at 2 days, due to the filler effect, but with lower levels than the CEM I paste at later ages as reactive alumina was consumed.
C1100 showed more CH at all ages than all of the composite systems studied. The inert calcined sludge increases the effective water/cement ratio, enhancing clinker hydration. However, bound water contents were the lowest of those at 7 and 28 days, indicating that the filler effect does not compensate for clinker substitution. From 7 to 28 days, the CH content per unit cement in C825 and C1000 decreases as it is consumed by the pozzolanic reaction of the amorphous sludge present.

3.4.4 XRD Analysis

The incorporation of calcined sludge did not lead to the formation of new phases (Figure 11). The main difference in the XRD patterns was observed in the main peaks for CH, AFm and AFt. Rietveld refinement results are shown in Table 6. In the CEM I paste, over 80% of the alite reacted within 2 days and more than 90% reacted by 28 days. C825 inhibited alite hydration significantly. The presence of amorphous sludge reduced the peak intensity of CH confirming the previous findings that increased dissolved aluminium ions is related to the inhibition of alite hydration. The effect of sludge on alite hydration was less for C1000. However, C1100 accelerated alite hydration, due to the filler effect. In the C1100 paste, the aluminates are inert and have a filler effect. Both of these factors encourage enhanced alite hydration.

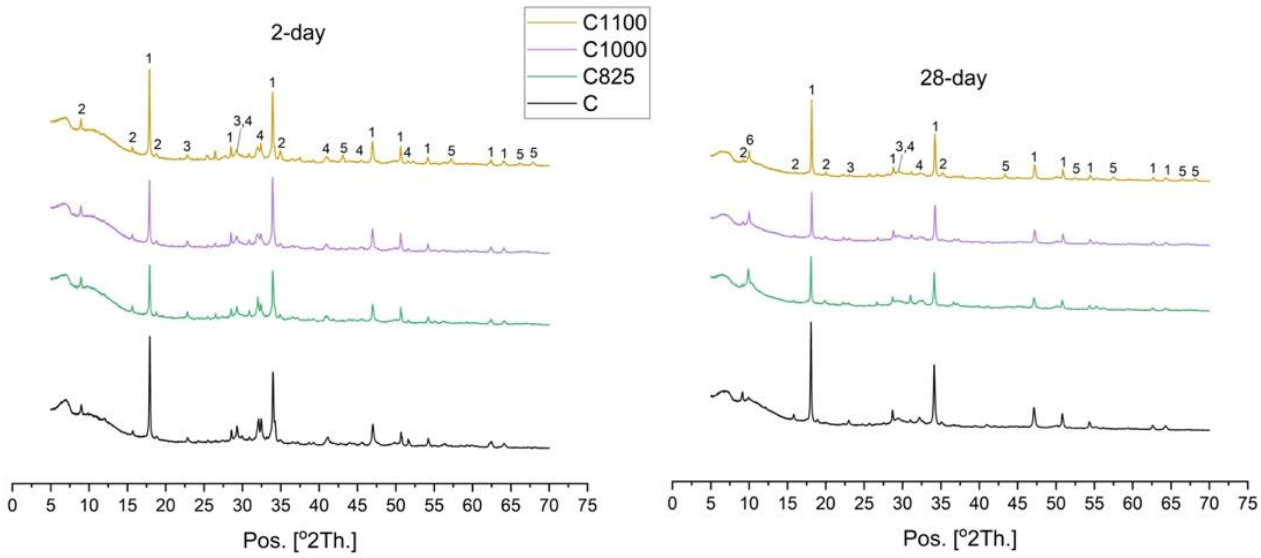

Figure 11: XRD patterns of hydrated pastes at (a) 2 days; (b) 28 days. The main peaks of 1: Portlandite; 2: Ettringite; 3: $CaCO_3$; 4:C_2S;C_3S; 5: Corundum; 6: Monosulfoaluminate.

In contrast, belite hydration is much slower but seemingly unaffected by the calcined sludges. C_3A was very reactive and was virtually consumed by 7 days in all pastes. The presence of amorphous sludge may accelerate C_3A hydration, since all was consumed within 2 days in the C825 paste. This is consistent with calorimetry results. Ferrite hydration was slightly accelerated in the presence of calcined sludge with about 80 to 90% reacted after 28 days of hydration.

At 2 days of hydration, the reduced amount CH in blended systems was accompanied with increased ettringite formation. This confirms calorimetry results which suggest that dissolved aluminium ions from the calcined sludge react with SO_4^{2-} and Ca^{2+} to produce ettringite. The dissolved Al^{3+} from the calcined sludge rapidly consume sulfate ions (gypsum) which accelerate C_3A hydration. At later ages, the ettringite content rapidly diminished, with production of AFm phase, monosulfoaluminate. Because of the higher amorphous content of sludge in C825 paste, this conversion occurred sooner, resulting in enhanced formation of AFm at the expense of AFt.

3.4.3 SEM analysis

The microstructures, observed by SEM-BSE imaging, of the neat system and C825 paste at 28 days are presented in Figure 12 (a) and (b) respectively. The images show the presence of partially hydrated cement particles, C-S-H, portlandite and pores. The higher degree of clinker hydration and CH content in the neat system is consistent with XRD and TG results. Image analysis of BSE images was used to determine the coarse porosity of cement pastes at 7 and 28 days and the results are presented in Figure 13. In addition to the degree of hydration, the physical characteristics of SCMs such as particle size, shape and density (Table 2) will also influence the compactness of the cement matrix. These physical properties are even more relevant where less reactive materials are incorporated in cement. From 7 to 28 days, the coarse porosity of all cement pastes decreased as hydration progressed. After 28 days, paste C825 showed a higher porosity than the CEM I paste, indicating that increased AFm formation does not compensate for the reduced degree of hydration. Sludge calcined at 825°C is irregularly shaped (Figure 6) so the filling effect will be slight. Incorporation of sludge calcined at 1000°C reduced porosity more than that calcined at 825°C, due to its smooth and rounded shape which enables better dispersion and space filling of the matrix. The addition of sludge calcined at 1100°C

further decreased porosity owing to the finer particle size. Because its particle was finer than the cement particles, its addition filled voids between cement particles, increasing the packing density.

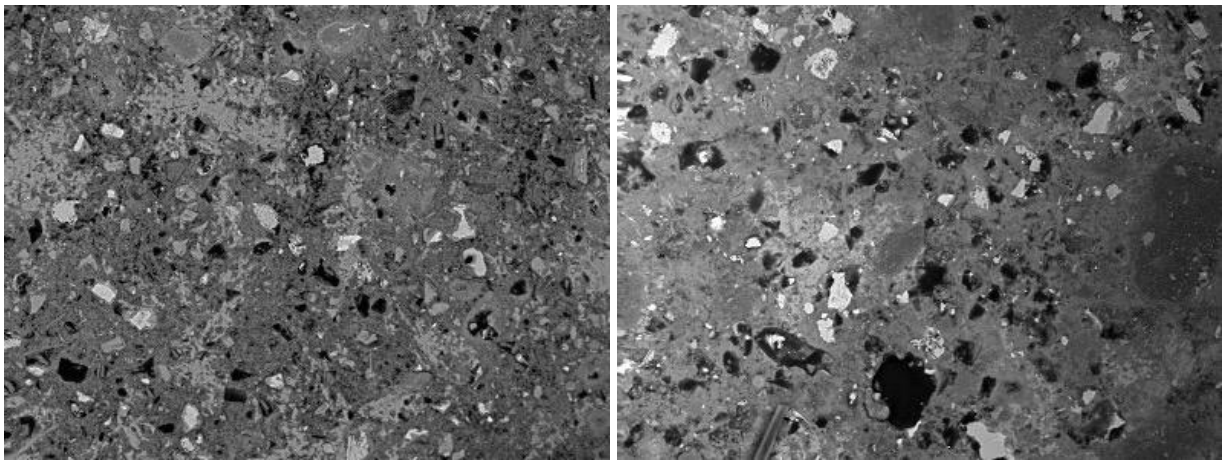

Figure 12: BSE micrographs at x800 magnification of a) OPC and b) C825 at 28 days of hydration

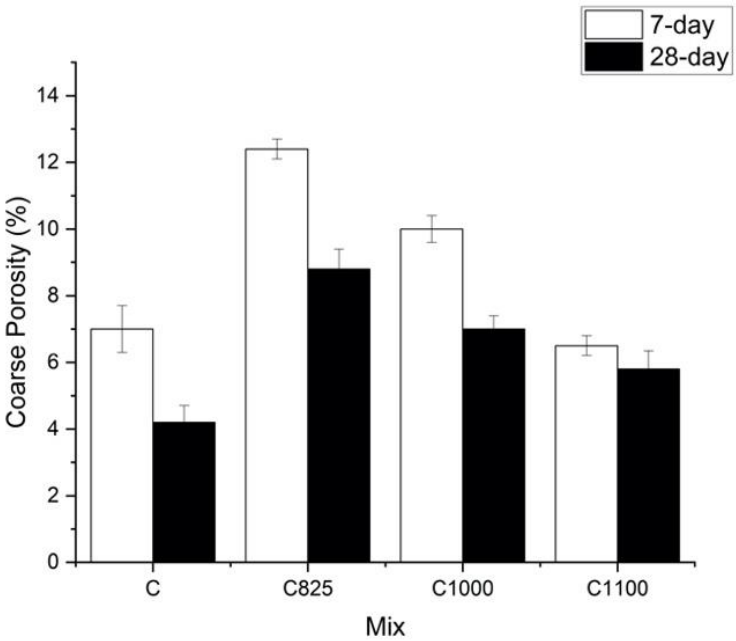

Figure 13: Coarse porosity of cement pastes at 7 and 28 days.

SEM-EDS analysis was then used to determine the elemental composition of the C-S-H. Figure 14 compares the Al/Ca and Si/Ca atomic ratios for the neat system and C825 paste. The Al/Si ratio of C-S-H is defined by the slope of a line drawn through the points with lowest Al/Ca ratio; while the Ca/Si ratio is taken as the point along this line at the high Si/Ca edge of the cloud of data points [62]. To minimise intermixing, only inner-product C-S-H was analysed. Table 7 summarizes the Ca/Si and Al/Si atomic ratios. The Ca/Si and Al/Ca ratios of the neat OPC system were ~1.88 and 0.06 respectively. All of the sludge-containing blends showed slightly reduced Ca/Si ratios and incorporation of aluminium into the C-S-H. Clinker replacement with sludge calcined at 825ºC resulted in increase in Al/Si ratio to ~0.10 and Ca/Si decreased to ~1.83. The blends containing more crystalline sludges showed slightly lower aluminium contents and slightly increased Ca/Si ratios. Thus, the amorphous calcined sludge (C825) led to an increase in the dissolved aluminium

concentration in pore solution, and so an increased Al/Si ratio [63]. The lower Ca/Si ratio in blended pastes is due to the additional Si, contributed by calcined sludge dissolution, [62,63]. Similar findings are well reported in the literature, where alumina-rich SCMs produce C-S-H with a lower Ca/Si and higher Al/Si ratios [62,63].

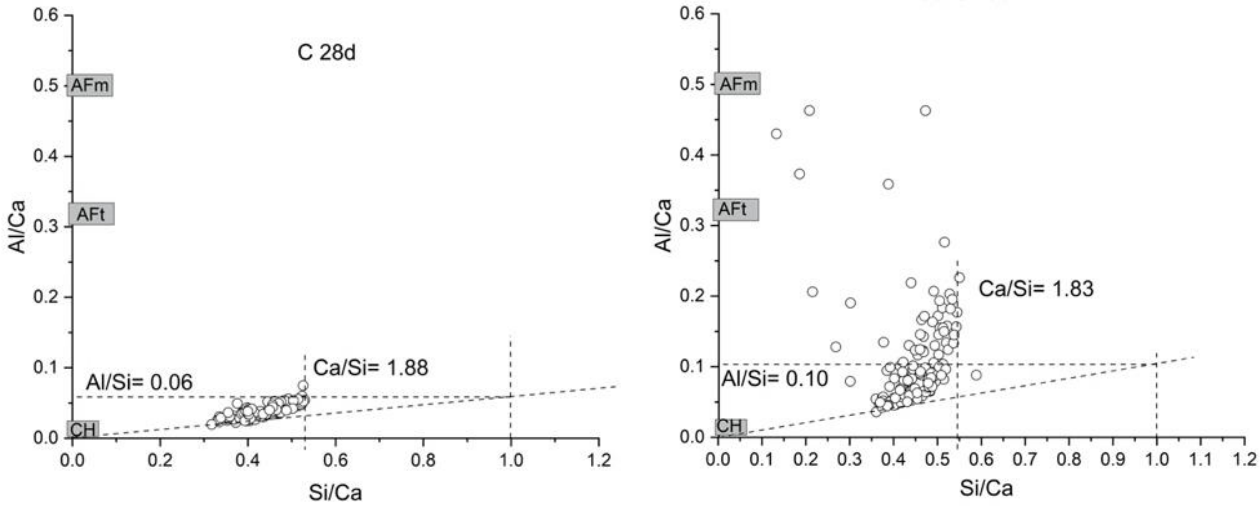

Figure 14: C-S-H composition for a) neat OPC and b) C825 at 28 days of hydration obtained by SEM-EDS (cloud of points and least intermixed composition).

Table 7: C-S-H composition for OPC and blended cement pastes at 28 days, obtained by SEM-EDS

	Al/Ca	Ca/Si
OPC	0.06	1.88
C825	0.10	1.83
C1000	0.07	1.85
C1100	0.06	1.85

3.5. Performance of blended cement mortars

3.5.1. Workability

The workability of fresh mortars is presented in Table 1. The variation in mortar flow was consistent with the morphological changes observed by SEM and changes in BET specific surface area. The mortar flow decreased with calcination temperature up to 825ºC and then increased with further increase in temperature. Up to a calcination temperature of 825ºC, the progressive agglomeration of irregular-shaped calcined sludge produced larger particles with increased SSA. Higher surface area will reduce the workability of blended cement mixtures. The very rapid initial reactivity of the 825ºC sludge, seen in the calorimetry data may also contribute to this reduction in workability. The first signs of sintering were observed at a calcination temperature of 1000ºC which resulted in rounded particles, a geometry that provides reduced external surface area, and thus improved workability.

3.5.2. Compressive strength

The pozzolanic activity of raw and calcined sludges was assessed by determining their strength activity indices (SAI). The index is defined as the ratio between strength of blended mortar (containing 20% SCM) and the strength in control mortar for a specific curing period. Figure 15 illustrates the SAI of raw and calcined sludges at 7 and 28 days of curing. The SAI of the sludge increases with calcination temperature. Replacement of cement with raw sludge gave zero strength.

This could be attributed to the sludge's 9.8% organic carbon content (Table 4). Organic carbon inhibits cement hydration by its adsorption onto hydration products, mainly C-S-H [64].

28 day SAI's for sludges calcined at 475ºC and 625ºC were 50.1% and 58.6% respectively. The increase in SAI could be attributed to the removal of organic carbon as characterization by XRD and FTIR showed that no new phases were formed at these temperatures. Calcination at 825ºC produced a more significant increase in 28-day SAI to 75.9%, attributed to the formation of poorly-crystalline η-alumina. Calcination of sludge at 1000ºC produced finer particles and well-crystallized η-alumina, giving an SAI of 77.1%. The increased fineness and reduced reactivity brought about by crystallization of the alumina suggests that the improvement in strength is mainly due to a filler effect. Calcining sludge at 1100ºC produced finer α-alumina particles, increasing the filler effect. The filler effect of the sludges calcined at 1000ºC and 1100ºC is supported by the reduced porosity and more compact microstructures observed by SEM analysis. In accordance with strength requirements of ASTM C618, the sludges calcined at 825ºC, 1000ºC and 1100ºC can be considered pozzolans as they meet the 75% SAI threshold. As a result, these samples were further characterized in pastes and mortars.

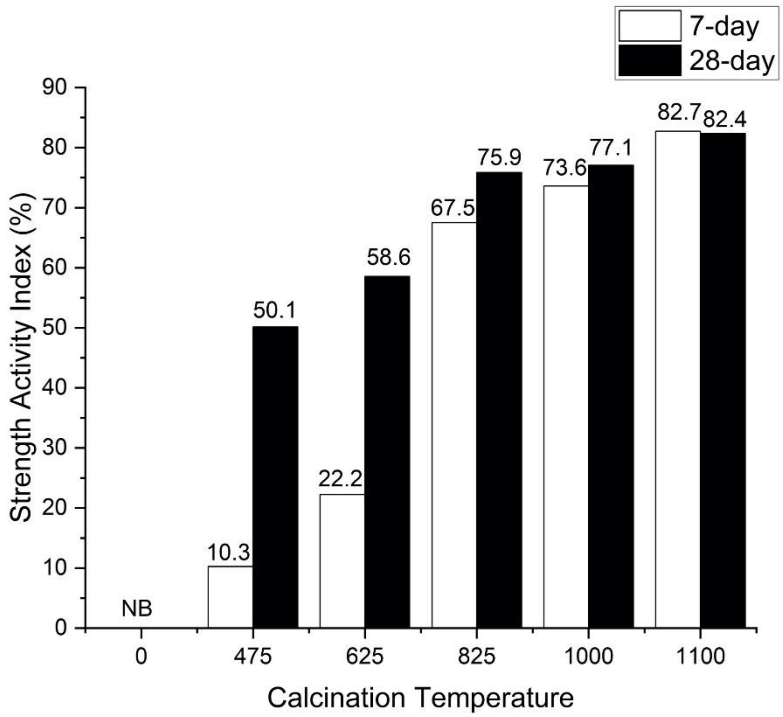

Figure 15: Strength Activity indices of raw and calcined sludges

Figure 16 shows the compressive strength of blended cement mortars at 2, 7 and 28 days. As indicated by the SAI values, the neat system produced the highest strength while the C825 paste produced the lowest strength at all ages. These differences can be explained based on the effects on cement hydration, as observed by thermal analysis, XRD and calorimetry. As α-alumina contained in the C1100 paste is unreactive, its incorporation in cement decreases the amount of cement clinker and the amount of hydration products. The lower amount of hydrates in C1100 paste explains why higher strength is observed in C1000 paste at 2 days of curing. The smaller density, larger particle size, spherical morphology of 1000ºC sludge enabled better space filling which translated to higher strength at early age. As cement hydration progress and more products are formed, the very fine sludge particles at 1100ºC had a better space filling effect which resulted in improved strength at 7 and 28 days.

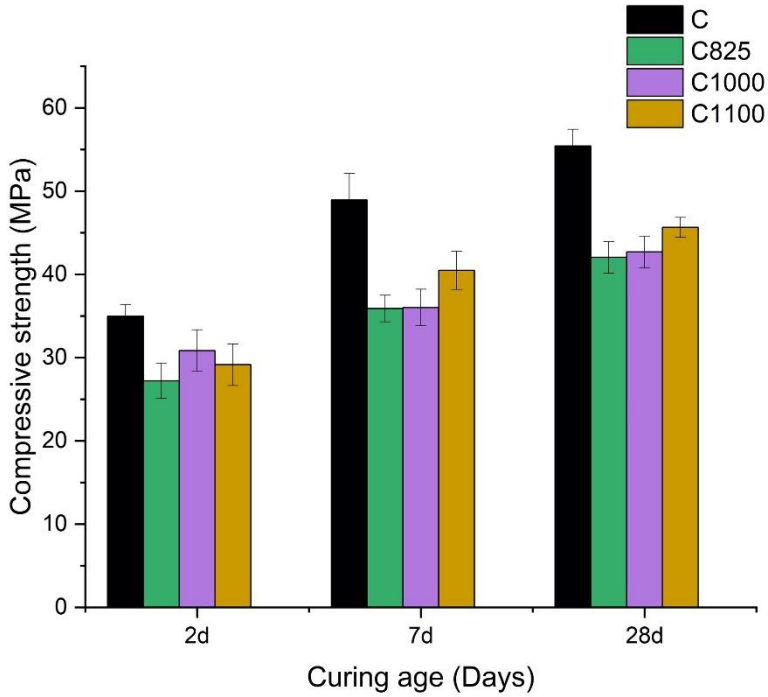

Figure 16: Strength development in cement mortars at 2, 7 and 28 days of curing.

The chemical and mineralogical variety of alum sludges results in differences in pozzolanic reactivity and mechanical strength in cement. Rodriguez et al. [12] studied the partial replacement of raw alum sludge with cement and found a substantial drop in strength with 28-day SAIs of 30 to 50%. This was attributed to the 5.1% organic carbon content in the raw sludge sample, whereas the higher organic carbon content of 9.8% in this study led to a non-binding effect on the cement matrix. In order to enhance pozzolanic reactivity, sludge samples reported in literature were calcined within the range 600-800ºC. Owaid et al. [4] and Gastaldini et al. [6] reported 7 and 28-day SAIs ranging from 98-125%. The improved performance in these studies was attributed to secondary C-S-H formed from the pozzolanic reaction between SiO_2 content in the calcined sludge and portlandite formed during cement hydration. However, the calcined sludge samples studied by Owaid et al. [4] and Gastaldini et al. [6] contained SiO_2 contents of 47.0 and 66.2%, and Al_2O_3 contents of 41.94 and 17.7% respectively. Meanwhile, the sludge sample collected in this study is mainly composed of Al_2O_3 (Table 3), with a significantly lower SiO_2 content. This limits its pozzolanic reactivity in cement. In addition, the higher Al_2O_3 content results in hindered alite hydration as observed by XRD and calorimetry. These factors result in the lower SAIs compared to previously reported studies.

4. Conclusions

This study investigated the effect of calcination on the physical, chemical and mineralogical properties of UK alum sludge and the effect of calcined alum sludge on the compressive strength and microstructure of blended cements. The main findings of this study are summarized as follows:

- The raw alum sludge is primarily an amorphous aluminium hydroxide precipitate with minor amounts of crystalline quartz and montmorillonite. In the temperature range 200-625ºC, there was no change in crystalline composition but significant mass loss was observed due to the dehydroxylation of $Al(OH)_3$ gel and the combustion of organic carbon. The formation of poorly-crystallized η-alumina (eta) occurs by 825ºC and crystallinity increased with temperature up to 1000ºC. At 1100ºC, the η-alumina transforms to highly-crystalline α-alumina, along with the formation other high temperature phases mullite and gehlenite.

- The above phase transitions were accompanied with morphological changes. The raw sludge consists of very fine, irregular particles which agglomerated with calcination temperature up to 825°C, developing internal porosity and increased surface area. At 1000°C, sintering occurs resulting in smooth, rounded particles with decreased BET surface area. At 1100°C, the complete removal of hydroxyl groups and formation of α-alumina led to the partial collapse of pore walls resulting in a drastic reduction in particle size and BET surface. The workability of fresh mortars varied consistently with changes in morphology and BET specific surface area. Higher surface area meant more water was adsorbed by the sludge particles which resulted in reduced workability. Thus, workability of corresponding mortars decreased with calcination temperature up to 825°C and then increases with further increase in temperature.
- Calcined alum sludge can be considered a pozzolan. Calcination temperature has a significant effect on the pozzolanic activity of alum sludge. Alum sludge calcined at 825°C showed the best reactivity due to the formation of poorly-crystallized η-alumina. With increasing calcination temperature to 1100°C, the reactivity decreased due to crystallization of alumina phases present. The calcined products derived at 1000°C and 1100°C showed a greater filler effect, and so led to greater strength development.
- Under alkaline conditions of cement paste, Al^{3+} ions dissolved from sludge calcined at 825°C are converted to $[Al(OH)_4]^-$ which are very reactive with Ca^{2+} and SO_4^{2-} ions, resulting in the early formation of ettringite. This reaction rapidly depletes gypsum and C_3A hydration takes place in an undersulfated system. C_3A consumes ettringite to form monosulfoaluminate after 3 hours. The rapid consumption of Ca^{2+} during the early formation of ettringite accelerates the onset of the silicate hydration peak. However, results suggest that the higher dissolution of η-alumina in C825 paste is related to the limited alite hydration which contributed to lower degrees of clinker hydration at later ages. This led to lower mortar compressive strengths in blends containing sludge calcined at 825°C. It is suggested that the early formed monosulfoaluminate covers up cement particles and reduces space available in the matrix. This decreases the rate and extent of alite hydration, resulting in lower compressive strength at later ages.
- The results of this study suggest that clinker hydration and mechanical strength are strongly influenced by Al_2O_3/SO_3 ratio in the calcined sludge-blended cements. To avoid an undersulfated condition, it is proposed that higher doses of gypsum and/ limestone powder can help control the accelerator effect of 825°C sludge on C_3A hydration. In this way, the higher reactivity of the 825°C sludge can be better utilized for improved performance. This study provides a fundamental base and a promising direction for further studies on proper utilization UK alum sludge as an SCM.

Acknowledgement

The authors would like to thank the Petroleum Technology Development Fund (PTDF) of Nigeria for funding this research. The research was undertaken in the Centre for Infrastructure Materials, University of Leeds, UK, a UKCRIC Research Facility (EP/P017169/1).

References

[1] Hart L D (LeRoy D . and Lense E 1990 *Alumina chemicals : science and technology handbook* (American Ceramic Society)

[2] U.S. EPA 2011 Drinking Water Treatment Plant Residuals. Management Technical Report. Summary of residuals generation, treatment and disposal at large community water systems. 378

[3] O'Kelly B C and Quille M E 2010 Shear strength properties of water treatment residues *Proc. ICE - Geotech. Eng.* **163** 23–35

[4] Owaid H M, Hamid R and Taha M R 2014 Influence of thermally activated alum sludge ash on the engineering properties of multiple-blended binders concretes *Constr. Build. Mater.* **61** 216–29

[5] Owaid H M, Hamid R and Taha M R 2019 Durability properties of multiple-blended binder concretes incorporating thermally activated alum sludge ash *Constr. Build. Mater.* **200** 591–603

[6] Gastaldini A L G, Hengen M F, Gastaldini M C C, do Amaral F D, Antolini M B and Coletto T 2015 The use of water treatment plant sludge ash as a mineral addition *Constr. Build. Mater.* **94** 513–20

[7] Gabriel L G G de, Rohden A B, Garcez M R, Costa E B da, Da Dalt S and Andrade J J de O 2019 Valorization of water treatment sludge waste by application as supplementary cementitious material *Constr. Build. Mater.* **223** 939–50

[8] Sales A, de Souza F R, dos Santos W N, Zimer A M and do Couto Rosa Almeida F 2010 Lightweight composite concrete produced with water treatment sludge and sawdust: Thermal properties and potential application *Constr. Build. Mater.* **24** 2446–53

[9] Sales A and de Souza F R 2009 Concretes and mortars recycled with water treatment sludge and construction and demolition rubble *Constr. Build. Mater.* **23** 2362–70

[10] Sales A, De Souza F R and Almeida F D C R 2011 Mechanical properties of concrete produced with a composite of water treatment sludge and sawdust *Constr. Build. Mater.* **25** 2793–8

[11] Husillos Rodríguez N, Martínez-Ramírez S, Blanco-Varela M T, Guillem M, Puig J, Larrotcha E and Flores J 2011 Evaluation of spray-dried sludge from drinking water treatment plants as a prime material for clinker manufacture *Cem. Concr. Compos.* **33** 267–75

[12] Rodríguez N H, Ramírez S M, Varela M T B, Guillem M, Puig J, Larrotcha E and Flores J 2010 Re-use of drinking water treatment plant (DWTP) sludge: Characterization and technological behaviour of cement mortars with atomized sludge additions *Cem. Concr. Res.* **40** 778–86

[13] Fernandez R, Martirena F and Scrivener K L 2011 The origin of the pozzolanic activity of calcined clay minerals: A comparison between kaolinite, illite and montmorillonite *Cem. Concr. Res.* **41** 113–22

[14] European Committee for Standardization. and British Standards Institution. 2007 Cement. Part 1, Composition, specifications and conformity criteria for common cements. 47

[15] Anon 2016 BSI Standards Publication Methods of testing cement Part 1 : Determination of strength

[16] LOTHENBACH B, DURDZIÑSKI P and DE WEERDT K 2015 Thermogravimetric analysis *A Practical Guide to Microstructural Analysis of Cementitious Materials* (CRC Press) pp 177–212

[17] Anon BS ISO 9277:2010 - Determination of the specific surface area of solids by gas adsorption. BET method

[18] Sun Z-X, Zheng T-T, Bo Q-B, Du M and Forsling W 2008 Effects of calcination temperature on the pore size and wall crystalline structure of mesoporous alumina *J. Colloid Interface Sci.* **319** 247–51

[19] Rossen J E, Lothenbach B and Scrivener K L 2015 Composition of C-S-H in pastes with increasing levels of silica fume addition *Cem. Concr. Res.* **75** 14–22

[20] Scrivener K, Snellings R and Lothenbach B 2016 *A Practical Guide to Microstructural Analysis of Cementitious Materials*

[21] Kocaba V 2009 *Development and evaluation of methods to follow microstructural development of cementitious systems including slags*

[22] Anon BS EN 1015-3:1999 - Methods of test for mortar for masonry. Determination of consistence of fresh mortar (by flow table)

[23] ASTMC109 2016 /C109M-16a, Standard Test Method for Compressive Strength of Hydraulic Cement Mortars (Using 2-in. or [50-mm] Cube Specimens), ASTM International, West Conshohocken, PA,

[24] ASTM C618 ASTM C618 - 19 Standard Specification for Coal Fly Ash and Raw or Calcined Natural Pozzolan for Use in Concrete

[25] Teixeira S R, Santos G T A, Souza A E, Alessio P, Souza S A and Souza N R 2011 The effect of incorporation of a Brazilian water treatment plant sludge on the properties of ceramic materials *Appl. Clay Sci.* **53** 561–5

[26] Ramachandran V S (Vangipuram S 2002 *Handbook of thermal analysis of construction materials* (Noyes Publications)

[27] Rodríguez N H, Ramírez S M, Varela M T B, Guillem M, Puig J, Larrotcha E and Flores J 2010 Re-use of drinking water treatment plant (DWTP) sludge: Characterization and technological behaviour of cement mortars with atomized sludge additions *Cem. Concr. Res.* **40** 778–86

[28] Chikouche M A, Ghorbel E and Bibi M 2016 The possibility of using dredging sludge in manufacturing cements: Optimization of heat treatment cycle and ratio replacement *Constr. Build. Mater.* **106** 330–41

[29] Pradhan J K, Bhattacharya I N, Das S C, Das R P and Panda R K 2000 Characterisation of fine polycrystals of metastable η-alumina obtained through a wet chemical precursor synthesis *Mater. Sci. Eng. B Solid-State Mater. Adv. Technol.* **77** 185–92

[30] Bhattacharya I N, Gochhayat P K, Mukherjee P S, Paul S and Mitra P K 2004 Thermal decomposition of precipitated low bulk density basic aluminium sulfate *Mater. Chem. Phys.* **88** 32–40

[31] Wefers K and Misra C 1987 *Oxides and Hydroxides of Aluminum*

[32] Lim T T, Chu J and Goi M H 2006 Effects of cement on redistribution of trace metals and dissolution of organics in sewage sludge and its inorganic waste-amended products *Waste Manag.* **26** 1294–304

[33] BSI 2012 BS En 450-1 Fly ash for concrete. Definition, specifications and conformity criteria, British Standard Institution, UK. 34

[34] Alphonse P and Courty M 2005 Structure and thermal behavior of nanocrystalline boehmite *Thermochim. Acta* **425** 75–89

[35] Kazantsev S O, Lozhkomoev A S, Glazkova E A, Gotman I, Gutmanas E Y, Lerner M I and Psakhie S G 2018 Preparation of aluminum hydroxide and oxide nanostructures with controllable morphology by wet oxidation of AlN/Al nanoparticles *Mater. Res. Bull.* **104** 97–103

[36] Souza A D V and Salomão R 2016 Evaluation of the porogenic behavior of aluminum hydroxide particles of different size distributions in castable high-alumina structures *J. Eur. Ceram. Soc.* **36** 885–97

[37] Nogueira F G E, Asencios Y J O, Rodella C B, Porto A L M and Assaf E M 2016 Alternative route for the synthesis of high surface-area η-Al2O3/Nb2O5 catalyst from aluminum waste *Mater. Chem. Phys.* **184** 23–30

[38] Radonjić L, Srdić V and Nikolić L 1993 Relationship between the microstructure of boehmite gels and their transformation to alpha-alumina *Mater. Chem. Phys.* **33** 298–306

[39] Aldcroft B D, Bye G C and Hughes A 1969 Crystallisation Processes in Aluminium Hydroxide Gels. IV. Factors Influencing the Formation of the Crystalline Trihydroxides *J. Appl. Chem.* **19** 167–72

[40] Vieira S C, Ramos A S and Vieira M T 2005 Mullitization kinetics from silica-and alumina-rich wastes

[41] Temuujin J, Jadambaa T, Mackenzie K J D, Angerer P, Porte F and Riley F 2000 Thermal formation of corundum from aluminium hydroxides prepared from various aluminium salts *Bull. Mater. Sci.* **23** 301–4

[42] Fernandez R, Martirena F and Scrivener K L 2011 The origin of the pozzolanic activity of calcined clay minerals: A comparison between kaolinite, illite and montmorillonite *Cem. Concr. Res.* **41** 113–22

[43] Tironi A, Trezza M A, Scian A N and Irassar E F 2013 Assessment of pozzolanic activity of

different calcined clays
[44] Zhang N, Liu X, Sun H and Li L 2011 Evaluation of blends bauxite-calcination-method red mud with other industrial wastes as a cementitious material: Properties and hydration characteristics *J. Hazard. Mater.* **185** 329–35
[45] Sembiring S, Simanjuntak W, Manurung P, Asmi D and Low I M 2014 Synthesis and characterisation of gel-derived mullite precursors from rice husk silica *Ceram. Int.* **40** 7067–72
[46] Madejová J 2003 FTIR techniques in clay mineral studies *Vib. Spectrosc.* **31** 1–10
[47] Danner T, Norden G and Justnes H 2018 Characterisation of calcined raw clays suitable as supplementary cementitious materials *Appl. Clay Sci.* **162** 391–402
[48] Ilić B, Radonjanin V, Malešev M, Zdujić M and Mitrović A 2016 Effects of mechanical and thermal activation on pozzolanic activity of kaolin containing mica *Appl. Clay Sci.* **123** 173–81
[49] Chakchouk A, Trifi L, Samet B and Bouaziz S 2009 Formulation of blended cement: Effect of process variables on clay pozzolanic activity *Constr. Build. Mater.* **23** 1365–73
[50] Kumara C K, Ng W J, Bandara A and Weerasooriya R 2010 Nanogibbsite: Synthesis and characterization *J. Colloid Interface Sci.* **352** 252–8
[51] Oréfice R L and Vasconcelos W L 1997 Sol-Gel transition and structural evolution on multicomponent gels derived from the alumina-silica system *J. Sol-Gel Sci. Technol.* **9** 239–49
[52] Maltese C, Pistolesi C, Bravo A, Cella F, Cerulli T and Salvioni D 2007 Effects of setting regulators on the efficiency of an inorganic acid based alkali-free accelerator reacting with a Portland cement *Cem. Concr. Res.* **37** 528–36
[53] Yang R, He T, Guan M, Guo X, Xu Y, Xu R and Da Y 2020 Preparation and accelerating mechanism of aluminum sulfate-based alkali-free accelerating additive for sprayed concrete *Constr. Build. Mater.* **234**
[54] Salvador R P, Cavalaro S H P, Segura I, Figueiredo A D and Pérez J 2016 Early age hydration of cement pastes with alkaline and alkali-free accelerators for sprayed concrete
[55] Salvador R P, Cavalaro S H P, Cincotto M A and Figueiredo A D d. 2016 Parameters controlling early age hydration of cement pastes containing accelerators for sprayed concrete *Cem. Concr. Res.* **89** 230–48
[56] Quennoz A and Scrivener K L 2013 Interactions between alite and C3A-gypsum hydrations in model cements *Cem. Concr. Res.* **44** 46–54
[57] Tan H, Li M, Ren J, Deng X, Zhang X, Nie K, Zhang J and Yu Z 2019 Effect of aluminum sulfate on the hydration of tricalcium silicate *Constr. Build. Mater.* **205** 414–24
[58] Herrera-Mesen C, Salvador R P, Cavalaro S H P and Aguado A 2018 Effect of gypsum content in sprayed cementitious matrices: Early age hydration and mechanical properties
[59] Begarin F, Garrault S, Nonat A and Nicoleau L 2011 Hydration of alite containing aluminium *Advances in Applied Ceramics* vol 110 pp 127–30
[60] Nicoleau L, Schreiner E and Nonat A 2014 Ion-specific effects influencing the dissolution of tricalcium silicate *Cem. Concr. Res.* **59** 118–38
[61] Chappex T and Scrivener K L 2012 The influence of aluminium on the dissolution of amorphous silica and its relation to alkali silica reaction *Cem. Concr. Res.* **42** 1645–9
[62] Deschner F, Winnefeld F, Lothenbach B, Seufert S, Schwesig P, Dittrich S, Goetz-Neunhoeffer F and Neubauer J 2012 Hydration of Portland cement with high replacement by siliceous fly ash *Cem. Concr. Res.* **42** 1389–400
[63] L'Hôpital E, Lothenbach B, Le Saout G, Kulik D and Scrivener K 2015 Incorporation of aluminium in calcium-silicate-hydrates *Cem. Concr. Res.* **75** 91–103
[64] Carlton W 1987 A review of solidification/stabilization interferences *J. Hazard. Mater.* **14** 5–21
[65] De Carvalho Gomes S, Zhou J L, Li W and Long G 2019 Progress in manufacture and properties of construction materials incorporating water treatment sludge: A review *Resour.*

Conserv. Recycl. **145** 148–59